Compression of FeSi, Fe_3C, $Fe_{0.95}O$, and FeS under the core pressures and implication for light element in the Earth's core

Nagayoshi Sata,[1,2] Kei Hirose,[1,3] Guoyin Shen,[2,4] Yoichi Nakajima,[3,5] Yasuo Ohishi,[6] and Naohisa Hirao[6]

Received 11 September 2009; revised 17 March 2010; accepted 29 April 2010; published 10 September 2010.

[1] The light alloying element in the Earth's core has not been identified yet. Here we determined the pressure-volume equations of state of FeSi, Fe_3C, and $Fe_{0.95}O$ in the core pressure range by a combination of diamond-anvil cell and synchrotron X-ray diffraction techniques. Both B2-type FeSi and Fe_3C cementite were preserved to 180 and 187 GPa, respectively. The rhombohedrally-distorted B1 phase of $Fe_{0.95}O$ was measured up to 186 GPa, and the distorted B8-type $Fe_{0.95}O$ was observed between 170 and 226 GPa. Combined with our previous data on FeS VI and B2-type VII phases to 270 GPa, we discuss the light element in the outer core by comparing the densities and compressibilities of these iron compounds with seismologically-estimated density profile in the core. Substitution of light element, particularly carbon and oxygen, in iron not only reduces the density but also enhances the compressibility remarkably. The core profile is therefore not reconciled with Fe-C and Fe-O compounds, while the densities and compressibilities of Fe-Si and Fe-S alloys match the observations. Carbon and oxygen may not be a predominant light element in the Earth's outer core, leaving silicon and sulfur as strong candidates.

Citation: Sata, N., K. Hirose, G. Shen, Y. Nakajima, Y. Ohishi, and N. Hirao (2010), Compression of FeSi, Fe_3C, $Fe_{0.95}O$, and FeS under the core pressures and implication for light element in the Earth's core, *J. Geophys. Res.*, *115*, B09204, doi:10.1029/2009JB006975.

1. Introduction

[2] *Birch* [1952] first realized that the density of the Earth's outer core is substantially lower than that of pure iron at core pressure and temperature (*P-T*). The outer core is therefore thought to contain considerable amount of one or more light elements such as silicon, carbon, oxygen, sulfur, and hydrogen (see reviews by *Poirier* [1994] and *Li and Fei* [2003]). While the density and seismic velocity profiles in the core and the properties of iron-rich alloys have been determined much more precisely to date [e.g., *Dziewonski and Anderson*, 1981; *Badro et al.*, 2007], the identification of light element(s) still remains uncertain. This is in large part because most of the previous experimental studies on iron–light element compounds were carried out at low pressures compared to the Earth's core (>136 GPa) and consequently the comparison of such experimental results with the observation was difficult.

[3] Here we studied the pressure-volume (*P-V*) relationships of FeSi to 180 GPa, Fe_3C to 187 GPa, and $Fe_{0.95}O$ to 226 GPa. The data on FeS have been also obtained to 270 GPa using the similar experimental techniques and reported elsewhere [*Ohfuji et al.*, 2007; *Sata et al.*, 2008]. These pressure ranges are much greater than those in earlier experimental studies. Using these *P-V* data, here we try to identify possible light element in the core. It is noted that the incorporation of light element reduces the density of iron but changes its compressibility simultaneously. The liquid outer core is most likely to be chemically uniform. Therefore, the pressure-density relationship of an iron-rich alloy with a certain chemical composition must be consistent with the density profile in the whole outer core deduced from seismological observations [*Dziewonski and Anderson*, 1981].

[4] In addition, there has been an extensive debate on the accuracy of pressure scales (equation of state of internal pressure standard), from which pressure is calculated in synchrotron X-ray diffraction (XRD) measurement. Simply due to the inconsistency between the different pressure scales, the pressure value can change by as much as 20 GPa at 100 GPa [e.g., *Hirose et al.*, 2008]. In this study, pressures were obtained by using several different pressure standards of MgO, Ar, and B2-type NaCl. We use the previous experimental data on pure iron by *Dubrovinsky*

[1]Institute for Research on Earth Evolution, Japan Agency for Marine-Earth Science and Technology, Yokosuka, Japan.
[2]Consortium for Advanced Radiation Sources, University of Chicago, Chicago, Illinois, USA.
[3]Department of Earth and Planetary Sciences, Tokyo Institute of Technology, Tokyo, Japan.
[4]Now at High Pressure Collaborative Access Team, Geophysical Laboratory, Carnegie Institution of Washington, Argonne, Illinois, USA.
[5]Now at Bayerishes Geoinstitut, Unversität Bayreuth, Bayreuth, Germany.
[6]SPring-8, Japan Synchrotron Radiation Research Institute, Sayo, Japan.

Copyright 2010 by the American Geophysical Union.
0148-0227/10/2009JB006975

et al. [2000], in which pressure was calculated by the Pt scale. In order to check the consistency between these pressure scales, we have conducted the simultaneous volume measurements of Ar, B2-NaCl, MgO, Au, and Pt up to 198 GPa in this study.

2. Experimental Methods

2.1. Measurements of Iron Compounds at Room Temperature

[5] The synchrotron XRD measurements were conducted at high pressures using a diamond-anvil cell (DAC) at BL10XU of SPring-8 [*Ohishi et al.*, 2008]. The reagent-grade FeSi powder (99.9% purity from Kojundo Chemical Lab. Co. Ltd) and the synthesized polycrystalline samples of Fe_3C and $Fe_{0.95}O$ were used for starting materials. A culet size of the diamond-anvil was 300-μm for experiments below 70 GPa, 90-μm for those below 190 GPa, and 60-μm for higher pressures (Table 1). The rhenium gasket was pre-indented down to the thickness equivalent to one sixth of the culet size, and subsequently a hole with a diameter of one third of the culet size was drilled at the center of the indentation as a sample chamber. The pelletized FeSi and Fe_3C samples were placed between the MgO pressure medium (99.99% purity). MgO was not used for experiments on $Fe_{0.95}O$ in order to avoid chemical reaction between them. Alternatively, argon (99.999% purity) was loaded at 190 MPa using high-pressure gas apparatus as the pressure medium for $Fe_{0.95}O$. Before loading argon, the DAC was dried in a vacuum oven for 30 min. The DAC using the MgO medium was also dried in the vacuum oven right before the compression in order to eliminate the moisture. The measurements of FeS have been conducted in Ar or MgO pressure medium using similar experimental methods [*Ohfuji et al.*, 2007; *Sata et al.*, 2008].

[6] The sample was compressed stepwise in the DAC. After each pressure increment, we heated the sample from both sides by a neodymium-doped yttrium-lithium-fluoride (Nd:YLF) laser to less than 1300 K for 15 to 30 min. This procedure minimizes the differential stress in the sample. After such thermal annealing, the XRD pattern of the sample was obtained at high pressure and room temperature. A monochromatic X-ray beam with a wavelength of *ca.* 0.4133 Å (30 keV) was collimated to 15- or 20-μm in diameter. Angle-dispersive XRD spectra were collected on an imaging plate (IP) detector or a charge coupled device (CCD) detector with a typical exposure time of 10 and 1 min, respectively. The 'FIT2D' program was employed for integrating the two-dimensional pattern into caked two-dimensional image and one-dimensional diffraction profile [*Hammersley et al.*, 1996]. Pressure was calculated from the volume of the pressure medium using its *P-V* equation of state; MgO [*Speziale et al.*, 2001] for FeSi and Fe_3C, and Ar [*Jephcoat*, 1998] for $Fe_{0.95}O$. Both MgO and Ar were used for experiments on FeS [*Ohfuji et al.*, 2007; *Sata et al.*, 2008].

2.2. High-Temperature Experiments

[7] Additionally a quasi-isothermal high-temperature compression experiment has been conducted on $Fe_{0.95}O$ at 1500 ± 150 K ($Fe_{0.95}O$ run#2) at the 13-ID-D experimental hatch at the Advanced Photon Source [*Shen et al.*, 2001] (Table 1). We used the diamond anvils with 150-μm and the stainless steel-guided boron gasket for this run. The sample was sandwiched between the reagent-grade NaCl layers, which served as a thermal insulator and a pressure standard. We repeated the heating cycles with increasing pressure. After the collection of XRD data at 1500 K, the sample was quenched to room temperature and further compressed in the DAC. The XRD collection time was 3 to 5 min.

[8] Pressure was estimated from the B2 phase of NaCl [*Sata et al.*, 2002], whose equation of state was obtained being based on the MgO scale proposed by *Speziale et al.* [2001]. However, NaCl was loaded as a pressure medium, in which very large temperature gradient should have existed during laser-heating. We therefore calculated the pressure from the volume of NaCl measured at 300 K after quenching temperature. The pressure at 1500 K may be higher by 5 to 10 GPa due to a contribution of thermal pressure.

2.3. Simultaneous Volume Measurements of Several Pressure Markers

[9] The volumes of several different pressure standards were measured simultaneously at high pressure using similar experimental techniques (Table 2). In run PM#1, a mixture of Au and NaCl (1:7 by weight) was placed in an Ar pressure medium in the DAC. The Pt and NaCl mixture (1:7 by weight) was compressed in the Ar and MgO pressure medium in run PM#2 and PM#3, respectively. Similarly to the experiments on iron compounds, the sample was thermally annealed by a Nd:YLF laser for 15 to 30 min after each pressure increment. Subsequently the XRD data were collected at room temperature.

3. Results

[10] We have conducted two runs each for FeSi, Fe_3C, and $Fe_{0.95}O$. Additional three runs were also carried out to check the consistency between the different pressure markers. The observed unit-cell parameters and volumes of the sample and coexisting pressure standard are summarized in Tables 1 and 2. The deviatoric stress (non-hydrostaticity) should not have been significant even at ~200 GPa, because thermal annealing was performed repeatedly with increasing pressure. It is supported by the fact that the uncertainties in measured unit-cell parameters of Fe_3C, for instance, were not enhanced with increasing pressure to 193 GPa (Table 1).

3.1. FeSi

[11] The volume of FeSi was measured in a pressure range from 26 to 180 GPa (Figure 1). The B2 phase (CsCl-type) of FeSi was synthesized from ε-FeSi (B20 phase) upon the first heating of each run and was preserved to 180 GPa. The caked two-dimensional diffraction image and the integrated one-dimensional spectrum are shown in Figure 2. No evidence of chemical reaction was observed in diffraction data. Observed peak positions and the result of unit-cell refinement are listed in Table 3. The volume after releasing the press load was also obtained in the first run. The results of two separate runs were consistent with each other. While the volume of the B2 phase was observed to be smaller by about 5% than that of ε-FeSi at equivalent pressure, both exhibit a

Table 1. Observed Unit-Cell Parameters and Volumes of Iron Compounds[a]

	FeSi (B2, Z = 1)				MgO (B1, Z = 4)			
Run Number	*a* (Å)	*b* (Å)	*c* (Å)	Volume (Å^3/unit-cell)	*a* (Å)	Volume (Å^3/unit-cell)	Pressure[b] (GPa)	V_{Si}/V_{Fe}
FeSi #1								
13	2.68758(26)			19.4125(56)	4.03812(46)	65.847(23)	25.93(9)	0.9554(6)
21	2.65828(25)			18.7847(53)	3.98272(45)	63.174(22)	37.48(10)	0.9611(6)
31	2.62743(25)			18.1382(51)	3.92628(44)	60.526(21)	51.31(12)	0.9633(6)
52	2.60563(24)			17.6905(49)	3.88744(58)	58.748(27)	62.22(17)	0.9626(5)
54	2.58062(24)			17.1858(48)	3.84267(57)	56.741(26)	76.41(19)	0.9615(5)
65	2.57510(24)			17.0759(47)	3.83410(57)	56.363(25)	79.33(20)	0.9595(5)
82	2.55523(23)			16.6836(46)	3.79996(56)	54.870(25)	91.74(21)	0.9564(5)
97	2.54517(23)			16.4873(45)	3.78210(55)	54.100(24)	98.72(22)	0.9554(5)
111	2.77211(23)			21.3027(53)	4.20559(50)	74.384(27)	0.62(6)	
FeSi #2								
24	2.54567(23)			16.4970(45)	3.78078(41)	54.044(18)	99.27(17)	0.9582(5)
32	2.51961(29)			15.9956(55)	3.73540(40)	52.121(17)	118.72(19)	0.9540(7)
42	2.49524(39)			15.5358(73)	3.69768(39)	50.558(17)	136.89(20)	0.9438(9)
56	2.46860(28)			15.0437(51)	3.65137(52)	48.682(21)	162.01(31)	0.9385(7)
73	2.45230(27)			14.7476(49)	3.62183(51)	47.510(21)	179.85(33)	0.9367(6)

	Fe_3C (Z = 4)				MgO (B1, Z = 4)			
Run Number	*a* (Å)	*b* (Å)	*c* (Å)	Volume (Å^3/unit-cell)	*a* (Å)	Volume (Å^3/unit-cell)	Pressure[b] (GPa)	V_C/V_{Fe}
Fe_3C #1								
29	4.24773(68)	4.84304(79)	6.35837(64)	130.804(30)	3.9321(11)	60.797(50)	49.87(28)	0.5273(8)
45	4.18121(76)	4.77308(78)	6.27529(63)	125.238(30)	3.8649(12)	57.732(55)	69.21(39)	0.5241(8)
Fe_3C #2								
56	4.16139(77)	4.75747(69)	6.2672(15)	124.076(30)	3.84016(58)	56.630(26)	77.32(20)	0.5465(8)
83	4.11026(80)	4.70626(90)	6.1819(16)	119.583(33)	3.77704(56)	53.883(24)	100.78(23)	0.5571(10)
111	4.04856(73)	4.64267(66)	6.1073(14)	114.794(27)	3.72230(54)	51.575(23)	124.81(26)	0.5350(8)
130	4.02151(78)	4.61128(67)	6.0563(14)	112.311(27)	3.68896(54)	50.201(22)	141.37(28)	0.5325(9)
151	3.99268(72)	4.57794(70)	6.0112(14)	109.874(26)	3.65638(53)	48.883(22)	159.13(30)	0.5283(8)
172	3.96141(78)	4.54611(82)	5.9607(14)	107.347(27)	3.62515(52)	47.641(21)	177.77(32)	0.5167(9)
193	3.94656(69)	4.53255(63)	5.9509(14)	106.449(25)	3.61127(52)	47.096(21)	186.60(33)	0.5185(8)

	$Fe_{0.95}O$ (rhombohedral B1, Z = 3)				Ar (fcc, Z = 4)			
Run Number	*a* (Å)	*b* (Å)	*c* (Å)	Volume (Å^3/unit-cell)	*a* (Å)	Volume (Å^3/unit-cell)	Pressure[c] (GPa)	V_O/V_{Fe}
FeO #1								
56	2.60519(54)		7.3655(25)	43.292(20)	3.71490(100)	51.267(40)	93.18(26)	0.7463(8)
73	2.56823(53)		7.1717(24)	40.965(18)	3.63129(92)	47.8831(37)	118.92(32)	0.7185(7)
90	2.54582(52)		7.0243(23)	39.426(18)	3.56569(89)	45.3346(34)	143.85(37)	0.7084(7)
102	2.52106(79)		6.9113(17)	38.042(20)	3.50750(90)	43.151(32)	170.20(42)	0.6986(9)
103	2.52039(79)		6.8790(16)	37.844(20)	3.50663(90)	43.119(32)	170.30(42)	0.6902(9)
138	2.4996(16)		6.8453(32)	37.039(20)	3.47670(84)	42.025(31)	186.00(45)	0.6814(9)

	$Fe_{0.95}O$ (orthorhombic B8, Z = 4)				Ar (fcc, Z = 4)			
Run Number	*a* (Å)	*b* (Å)	*c* (Å)	Volume (Å^3/unit-cell)	*a* (Å)	Volume (Å^3/unit-cell)	Pressure (GPa)[c]	V_O/V_{Fe}
FeO #1								
102	4.93206(89)	2.40774(92)	4.22116(94)	50.127(19)	3.50750(90)	43.151(32)	170.20(42)	0.6792(6)
103	4.93102(89)	2.40608(92)	4.22031(94)	50.072(19)	3.50663(90)	43.119(32)	170.30(42)	0.6776(6)
138	4.85521(86)	2.38784(90)	4.19008(93)	48.577(18)	3.47670(84)	42.025(31)	186.00(45)	0.6547(6)
168	4.84223(86)	2.36692(89)	4.15700(91)	47.644(18)	3.44731(83)	40.968(30)	202.40(48)	0.6488(6)
217	4.82738(86)	2.34892(87)	4.12722(90)	46.800(17)	3.41983(82)	39.996(29)	219.10(51)	0.6443(6)
265	4.81411(85)	2.33994(87)	4.11315(90)	46.334(17)	3.40883(81)	39.611(29)	226.14(53)	0.6380(6)

	$Fe_{0.95}O$ (B1, Z = 4)				NaCl (B2, Z = 1)			
Run Number	*a* (Å)	*b* (Å)	*c* (Å)	Volume (Å^3/unit-cell)	*a* (Å)	Volume (Å^3/unit-cell)	Pressure[d] (GPa)	V_O/V_{Fe}
FeO #2 (1500 K)								
10-9	4.0793(30)			67.88(15)	2.9455(13)	25.554(36)	42.0(2)	0.7717(38)
10-12	4.0146(32)			64.71(16)	2.8806(101)	23.903(26)	55.9(24)	0.7568(41)
10-15	3.9704(47)			62.59(23)	2.8367(14)	22.826(35)	67.7(4)	0.7491(60)
10-18	3.9445(60)			61.37(28)	2.8109(25)	22.208(60)	75.8(8)	0.7460(78)
12-07	3.9130(45)			59.91(21)	2.7858(26)	21.620(61)	84.5(9)	0.7351(58)
12-15	3.8851(82)			58.64(38)	2.7651(26)	21.141(60)	92.5(10)	0.7245(106)
12-18	3.8784(78)			58.34(36)	2.7616(40)	21.061(92)	94.0(16)	0.7202(101)
13-22	3.8668(40)			57.82(19)	2.7519(9)	20.839(20)	98.0(4)	0.7173(52)

Table 1. (continued)

	FeSi (B2, Z = 1)				MgO (B1, Z = 4)			
Run Number	*a* (Å)	*b* (Å)	*c* (Å)	Volume (Å^3/unit-cell)	*a* (Å)	Volume (Å^3/unit-cell)	Pressure[b] (GPa)	V_{Si}/V_{Fe}
13-32	3.8405(76)			56.65(34)	2.7331(15)	20.418(35)	106.4(7)	0.7071(99)
13-43	3.8053(64)			55.10(28)	2.7131(13)	19.970(30)	116.1(7)	0.6870(83)
13-49	3.7987(25)			54.82(11)	2.7028(39)	19.745(85)	121.5(20)	0.6918(32)
13-65	3.7977(54)			54.77(24)	2.7003(31)	19.689(68)	122.8(16)	0.6938(71)
13-74	3.7804(153)			54.03(66)	2.6892(15)	19.448(32)	128.9(8)	0.6858(198)
13-81	3.7797(87)			54.00(38)	2.6893(35)	19.450(77)	128.9(20)	0.6848(113)
13-100	3.7778(74)			53.54(42)	2.6772(10)	19.189(22)	135.9(6)	0.6870(128)
14-19	3.7679(16)			53.01(28)	2.6723(7)	19.083(14)	138.8(4)	0.6772(86)

Run Number	Volume (Å^3/unit-cell)	Pressure[b,c] (GPa)	V_S/V_{Fe}
	FeS (VI, Z = 4)		
FeS[e]			
1-38	76.71(3)	68.9(4)	1.1572(8)
1-69	73.56(3)	84.8(4)	1.1312(9)
2-40	71.30(3)	101.1(2)	1.1219(9)
2-62	76.22(2)	70.3(1)	1.1495(6)
3-108	82.92(3)	39.0(1)	1.1736(8)
3-140	81.74(3)	44.3(1)	1.1735(8)
4-51	69.94(6)	112.3(5)	1.1166(18)
4-63	68.25(6)	130.6(5)	1.1179(16)
4-73	66.49(5)	148.5(6)	1.1095(16)
4-84	64.71(5)	170.5(6)	1.1039(16)
4-100	62.92(5)	185.5(6)	1.0774(17)
4-119	62.30(5)	198.2(6)	1.0825(17)
4-139	61.31(5)	214.5(6)	1.0801(17)
	FeS (VII, Z = 1)		
FeS[e]			
4-100	15.193	185.5(6)	1.0065
4-119	15.051	198.2(6)	1.0124
4-139	14.825	214.5(6)	1.0119
4-141	13.97	270.4(8)	0.9836
4-145	14.4971(67)	232.7(7)	0.9985(9)
4-164	14.4195(67)	236.6(7)	0.9943(9)

[a]Numbers in parentheses represent errors in the last digits.
[b]Estimated by EoS of MgO [*Speziale et al.*, 2000] (V_0 = 74.71 Å^3/unit-cell, K_0 = 160.2 GPa, and K'_0 = 3.99 in BM3EoS).
[c]Estimated by EoS of Ar [*Jephcoat*, 1998] (V_0 = 149.8 Å^3/unit-cell, K_0 = 3.3 GPa, and K'_0 = 7.24 in Vinet EoS [*Vinet et al.*, 1986]).
[d]Estimated by EoS of B2-NaCl [*Sata et al.*, 2002] at 300 K after heating (V_r = 27.17 Å^3/unit-cell, P_r = 32.08 GPa, K_r = 143.2 GPa, and K'_r = 3.94 in mBM3 EoS).
[e]From *Ohfuji et al.* [2007] and *Sata et al.* [2008].

similar compressibility below 50 GPa [*Knittle and Williams*, 1995, *Lin et al.*, 2003].

[12] These *P*-*V* data to 180 GPa are fitted to the 3rd-order modified Birch-Murnaghan equation of state (here after, mBM3 EoS) [*Sata et al.*, 2002]:

$$P = \left\{ P_r - \frac{1}{2}(3K_r - 5P_r)\left[1 - \left(\frac{V}{V_r}\right)^{-2/3}\right] + \frac{9}{8}K_r\left(K_r' - 4 + \frac{35P_r}{9K_r}\right)\left[1 - \left(\frac{V}{V_r}\right)^{-2/3}\right]^2 \right\}\left(\frac{V}{V_r}\right)^{-5/3} \quad (1)$$

where subscripts *r* denote the values at reference point, V_r is a selected reference volume, and P_r, K_r, and K'_r are pressure, isothermal bulk modulus, and pressure dependence of the bulk modulus at the reference volume, respectively. The mBM3 does not require zero-pressure volume. It is similar to the '*g*-*G* analysis' by *Jeanloz* [1981], but strain *g* is not explicitly included in the formula. As a result, the fit does not depend on the choice of reference volume, V_r. The reference volume, V_r = 10.685 Å^3/atom (= 21.370 Å^3/unit-cell), gives the fitting results of $P_r = -0.01 \pm 0.47$ GPa, $K_r = 221.7 \pm 3.2$ GPa, and $K'_r = 4.167 \pm 0.063$. When we choose V_r giving P_r = 0 GPa, V_r, K'_r, and K'_r for the mBM3 EoS are identical to V_0, K'_0, and K'_0 for the 3rd-order Birch-Murnaghan EoS (BM3 EoS) [*Birch*, 1986]:

$$P = \frac{3}{2}K_0\left[\left(\frac{V}{V_0}\right)^{-7/3} - \left(\frac{V}{V_0}\right)^{-5/3}\right] \cdot \left\{1 + \frac{3}{4}\left(K_0' - 4\right)\left[\left(\frac{V}{V_0}\right)^{-2/3} - 1\right]\right\}. \quad (2)$$

Here, V_0, K'_0, and K'_0 are volume, bulk modulus, and pressure dependence of the bulk modulus, each at ambient pressure. The pressure-volume relationship of the B2 phase of FeSi is formulated by commonly used BM3 EoS with parameters of K_0 = 221.7 GPa, K'_0 = 4.167, and V_0 = 10.685 Å^3/atom (= 21.370 Å^3/unit-cell). The obtained compression curve of B2 FeSi is illustrated in Figure 1, together with that of hexagonal-close-packed (hcp) Fe reported by

Table 2. Measured Unit-Cell Parameters and Volumes of Au, Ar, NaCl, and Pt[a]

	Au (fcc, Z = 4)			Ar (fcc, Z = 4)			NaCl (B2, Z = 1)		
Run Number	*a* (Å)	Volume (Å^3/unit-cell)	Pressure[b] (GPa)	*a* (Å)	Volume (Å^3/unit-cell)	Pressure[c] (GPa)	*a* (Å)	Volume (Å^3/unit-cell)	Pressure[d] (GPa)
PM #1									
13	3.90663(44)	59.622(20)	30.95(11)	4.08324(47)	68.079(24)	30.96(5)	3.01518(26)	27.4120(71)	30.83(4)
22	3.87292(43)	58.092(20)	39.96(13)	3.99548(45)	63.783(22)	40.44(6)	2.95630(25)	25.8373(66)	40.04(5)
32	3.83264(42)	56.298(19)	52.41(15)	3.91855(44)	60.169(21)	50.97(7)	2.90232(37)	24.4476(95)	50.78(9)
43	3.81264(43)	55.421(19)	59.36(15)	3.86406(58)	57.676(26)	60.02(11)	2.86508(29)	23.5184(71)	59.79(8)
55	3.77510(41)	53.800(18)	73.92(17)	3.80392(42)	55.042(18)	71.64(9)	2.81866(28)	22.3938(67)	73.24(9)
65	3.75072(40)	52.765(18)	84.55(19)	3.77502(41)	53.796(18)	78.01(10)	2.78502(35)	21.6016(81)	84.83(13)
80	3.74346(40)	52.459(18)	87.92(20)	3.74346(40)	52.459(17)	85.59(11)	2.77768(34)	21.4313(80)	87.59(13)
88	3.72540(40)	51.703(17)	96.69(21)	3.69507(39)	50.451(17)	98.62(12)	2.75108(27)	20.8213(61)	98.38(12)
101	3.70605(40)	50.902(17)	106.78(22)	3.66807(39)	49.353(16)	106.71(13)	2.71991(32)	20.1216(72)	112.73(16)
113	3.68374(40)	49.988(16)	119.36(24)	3.63464(52)	48.016(21)	117.62(18)	2.70380(41)	19.7662(89)	120.95(22)
	Pt (fcc, Z = 4)			Ar (fcc, Z = 4)			NaCl (B2, Z = 1)		
	a (Å)	Volume (Å^3/unit-cell)	Pressure[e] (GPa)	*a* (Å)	Volume (Å^3/unit-cell)	Pressure[c] (GPa)	*a* (Å)	Volume (Å^3/unit-cell)	Pressure[d] (GPa)
PM #2									
14	3.79414(41)	54.618(18)	35.71(15)	4.02200(62)	65.062(31)	37.32(7)	2.97826(38)	26.417(11)	36.33(5)
22	3.75804(41)	53.074(18)	49.75(17)	3.91398(44)	59.959(21)	51.67(7)	2.90599(30)	24.5404(75)	49.97(6)
32	3.72788(40)	51.867(17)	63.17(19)	3.83321(42)	56.323(19)	65.70(8)	2.85233(29)	23.2059(70)	63.22(8)
40	3.68747(39)	50.140(16)	83.91(22)	3.74203(40)	52.399(17)	85.95(10)	2.78391(27)	21.5757(64)	85.25(10)
61	3.65601(39)	48.868(16)	102.50(24)	3.68452(53)	50.020(22)	101.71(16)	2.74013(26)	20.5738(60)	103.20(12)
73	3.63556(38)	48.052(16)	115.86(26)	3.64343(52)	48.365(21)	114.65(17)	2.71373(26)	19.9848(58)	115.81(13)
	Pt (fcc, Z = 4)			MgO (fcc, Z = 4)			NaCl (B2, Z = 1)		
	a (Å)	Volume (Å^3/unit-cell)	Pressure[e] (GPa)	*a* (Å)	Volume (Å^3/unit-cell)	Pressure[f] (GPa)	*a* (Å)	Volume (Å^3/unit-cell)	Pressure[d] (GPa)
PM #3									
35	3.72296(40)	51.602(17)	65.52(20)	3.87950(43)	58.388(20)	64.64(13)	2.84342(35)	22.9892(85)	65.73(10)
46	3.66589(39)	49.265(16)	96.41(24)	3.78489(41)	54.220(18)	97.52(17)	2.75239(33)	20.8511(75)	97.82(14)
68	3.62508(38)	47.638(15)	123.11(27)	3.72650(40)	51.749(17)	122.66(19)	2.69568(42)	19.5887(92)	125.32(23)
91	3.60085(38)	46.689(15)	141.05(30)	3.68921(39)	50.211(16)	141.03(21)	2.66451(41)	18.9169(88)	143.65(26)
117	3.58160(51)	45.944(20)	156.52(43)	3.66426(39)	49.199(16)	154.44(22)	2.64735(41)	18.5539(86)	154.86(28)
136	3.56696(50)	45.383(20)	169.05(45)	3.64202(38)	48.309(16)	167.22(23)	2.6246[g]	18.080	171.1
139	3.56703(50)	45.386(20)	169.00(45)	3.64365(38)	48.373(16)	166.26(23)	2.6243[g]	18.074	171.3
160	3.55471(50)	44.917(19)	180.08(47)	3.62325(38)	47.566(15)	178.64(24)	2.6100[g]	17.780	182.5
179	3.54193(50)	44.435(19)	192.13(48)	3.60823(38)	46.977(15)	188.23(25)	2.5962[g]	17.498	194.0
203	3.53562(50)	44.198(19)	198.29(49)	3.59760(38)	46.563(15)	195.26(26)	2.5920[g]	17.415	197.5

[a]Numbers in parentheses represent errors in the last digits.
[b]Estimated by EoS of Au [*Hirose et al.*, 2008] (V_0 = 67.85 Å^3/unit-cell, K_0 = 167 GPa, and K'_0 = 5.58 in BM3 EoS).
[c]Estimated by EoS of Ar [*Jephcoat*, 1998] (V_0 = 149.8 Å^3/unit-cell, K_0 = 3.3 GPa, and K'_0 = 7.24 in Vinet EoS).
[d]Estimated by EoS of NaCl B2 [*Sata et al.*, 2002] (V_r = 27.17 Å^3/unit-cell, P_r = 32.08 GPa, K_r = 143.2 GPa, and K'_r = 3.94 in mBM3 EoS).
[e]Estimated by EoS of Pt [*Holmes et al.*, 1989] (V_0 = 60.40 Å^3/unit-cell, K_0 = 266 GPa, and K'_0 = 5.81 in Vinet EoS).
[f]Estimated by EoS of MgO [*Speziale et al.*, 2001] (V_0 = 74.71 Å^3/unit-cell, K_0 = 160.2 GPa, and K'_0 = 3.99 in BM3 EoS).
[g]Estimated from 110 peak only.

Dubrovinsky et al. [2000]. We found that the B2 phase of FeSi is slightly more compressible than hcp Fe under core pressure (>135 GPa).

[13] The high-pressure B2 phase of FeSi was first synthesized by *Dobson et al.* [2002]. Its compression behavior was subsequently determined up to 40 GPa by *Dobson et al.* [2003] as V_0 = 10.87 Å^3/atom, K_0 = 184 GPa, and K'_0 = 4.2 using the BM3 EoS. *Ono et al.* [2007a] also reported V_0 = 10.66 Å^3/atom and K_0 = 225 GPa assuming K'_0 = 4 based on the experiments up to 67 GPa. Our observations are consistent with the result of *Ono et al.* [2007a], but the volumes were determined to be slightly smaller in this study above 50 GPa. The volumes observed by *Dobson et al.* [2003] below 20 GPa were larger than ours, which is likely due to the excess iron in Dobson's starting material. Theoretical calculations by *Vočadlo et al.* [1999] showed V_0 = 10.61 Å^3/atom, K_0 = 226 GPa, and K'_0 = 5.4 at T = 0 K. *Caracas and Wentzcovitch* [2004] gave V_0 = 10.687 Å^3/atom, K_0 = 220 GPa, and K'_0 = 4.796. Since these K'_0 values are much greater than that determined in our experiments (K'_0 = 4.17), both theoretical studies predict much larger volumes at megabar pressure range.

3.2. Fe_3C

[14] The Fe_3C cementite was observed throughout the present experiments up to 187 GPa (Table 1). The caked two-dimensional diffraction image and the integrated one-dimensional spectrum at 187 GPa are shown in Figure 3. Most of the peaks are assigned to Fe_3C and MgO. Minor peaks from Fe_7C_3 and Re (gasket material) were also observed in the diffraction patterns. The result of unit-cell refinement of Fe_3C at 187 GPa is given in Table 4. It is known that it undergoes a magnetic transition around 25 GPa [*Lin et al.*, 2004], which changes its elastic property. It is true that our data obtained above 50 GPa show a smaller

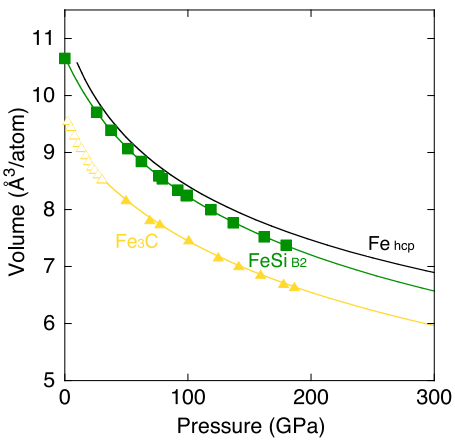

Figure 1. Observed volumes of FeSi and Fe_3C. Green squares, B2 phase of FeSi; yellow triangles, Fe_3C cementite (closed and open symbols are from this study and *Li et al.* [2003], respectively). Black solid curve represents the pressure-volume relation of hcp Fe by *Dubrovinsky et al.* [2000].

compressibility than that below 25 GPa [*Scott et al.*, 2001; *Li et al.*, 2002] (Figure 1).

[15] Combined with the previous data by *Li et al.* [2002] collected at greater than 25 GPa (Figure 1), the present *P-V* data are fitted to the mBM3 EoS. The fitting results give $P_r = 0.0 \pm 1.6$ GPa, $K_r = 290 \pm 13$ GPa, and $K'_r = 3.76 \pm 0.18$ with $V_r = 9.341$ Å^3/atom (= 149.46 Å^3/unit-cell). Previous spin-restricted calculations by *Vočadlo et al.* [2002] suggested the fairly small V_0 and large K'_0 for this nonmagnetic phase compared to our results.

3.3. $Fe_{0.95}O$

3.3.1. Orthorhombic B8 Phase

[16] We have performed room temperature and high temperature experiments in run #1 and #2, respectively (Table 1). At 300 K, only the rhombohedrally-distorted B1 phase (rB1) was observed between 93 and 144 GPa. This is consistent with the previous observations that the cubic B1 phase transformed to rB1 above 20 GPa at 300 K [*Shu et al.*, 1998; *Jacobsen et al.*, 2005, and references therein] and the rB1 phase was observed up to 142 GPa [*Ono et al.*, 2007b]. At 1500 K in run #2, only cubic B1 phase was observed up to the maximum pressure of 139 GPa, consistent with the previous reports [*Seagle et al.*, 2008; *Campbell et al.*, 2009]. The origin of apparent disagreement with other previous experimental data could be the difference in the stress state of the sample (the use of different pressure medium) or iron deficiency of $Fe_{1-X}O$ sample (possibly changed by coexisting with Fe metal) but is not clear [*Murakami et al.*, 2004; *Kondo et al.*, 2004; *Ozawa et al.*, 2010].

[17] The diffraction peaks from the NiAs-type (B8) phase first appeared at 170 GPa after laser-heating. The change in the observed XRD patterns between 144 and 226 GPa is shown in Figure 4. The caked two-dimensional diffraction image is also provided. The intensity of the B8 peaks became stronger with increasing pressure. The coexisting rB1 phase was preserved up to 186 GPa. We observed the splitting of the 100 and 102 peaks of the hexagonal B8 phase, and the splitting was enhanced when the pressure was increased. In contrast, the 002 peak did not split even at 226 GPa. Such peak splitting indicates a distortion to an orthorhombic symmetry (oB8). The observed peaks were indexed based on the orthorhombic unit-cell with lattice parameters of $a = 4.81411 \pm 0.00086$ Å, $b = 2.33994 \pm 0.00088$ Å, and $c = 4.11315 \pm 0.00090$ Å at 226 GPa (Table 5). The *c*/*b*

Table 3. Observed and Calculated X-Ray Diffraction Peaks of B2 Phase of FeSi at 180 GPa[a]

h	*k*	*l*	d_{obs}	d_{calc}	Δd
1	0	0	2.45435(14)	2.45230	0.00205
1	1	0	1.73348(10)	1.73404	−0.00056
1	1	1	1.41646(10)	1.41584	0.00062
2	0	0	1.22641(7)	1.22615	0.00026
2	1	0	1.09613(4)	1.09670	−0.00057

[a]Numbers in parentheses represent errors in the last digits. Lattice parameters of $a = 2.45230 \pm 0.00027$ Å were determined by using the UnitCell [*Holland and Redfern*, 1997].

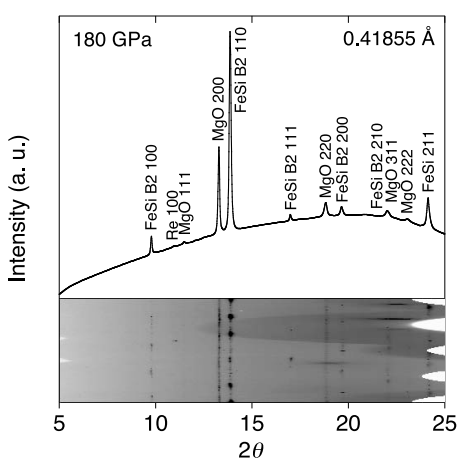

Figure 2. Caked 2D diffraction image and integrated 1D spectrum of B2 phase of FeSi at 180 GPa and 300 K.

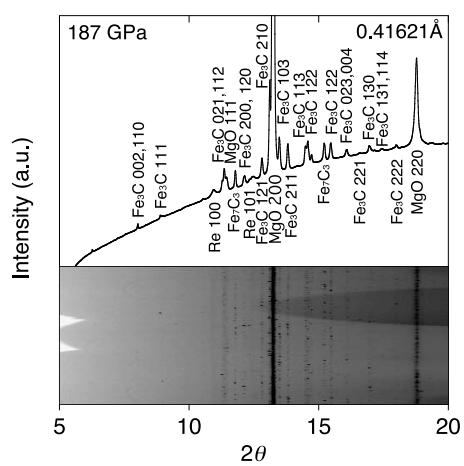

Figure 3. Caked 2D diffraction image and integrated 1D spectrum of Fe_3C at 187 GPa and 300 K. Observed peaks are mostly indexed by cementite structure of Fe_3C and MgO pressure medium. Some peaks from Fe_7C_3 and Re gasket were also observed.

Table 4. Observed and Calculated X-Ray Diffraction Peaks of Fe_3C at 193 GPa[a]

h	k	l	d_{obs}	d_{calc}	Δd
1	1	1	2.66086(61)	2.66200	−0.00114
2	0	0	1.97283(52)	1.97328	−0.00046
1	2	0	1.96541(52)	1.96529	0.00012
1	2	1	1.86532(6)	1.86616	−0.00084
1	0	3	1.77224(13)	1.77234	−0.00010
2	1	1	1.73097(5)	1.73102	−0.00005
1	1	3	1.65046(17)	1.65064	−0.00017
1	2	2	1.64002(15)	1.63987	0.00015
2	1	2	1.54669(4)	1.5459	0.00079
2	2	1	1.44366(27)	1.44374	−0.00008
1	3	0	1.41117(18)	1.41099	0.00018
1	3	1	1.37298(21)	1.37292	0.00006

[a]Numbers in parentheses represent errors in the last digits. Lattice parameters of a = 3.94656 ± 0.00069 Å, b = 4.53255 ± 0.00063 Å, and c = 5.95085 ± 0.00133 Å were determined by using the UnitCell [*Holland and Redfern*, 1997].

ratio, whose divergence from 1.732 of the ideal B8 structure indicates the degree of orthorhombic distortion, is 1.753 at 170 GPa to 1.758 at 226 GPa. *Fei and Mao* [1994] first experimentally observed the B8 phase of $Fe_{0.98}O$ with c/a = 2.01 at 96 GPa and 800 K, which is exceedingly large compared to that of ideal B8 structure. The orthorhombic cell observed in this study has the corresponding value of

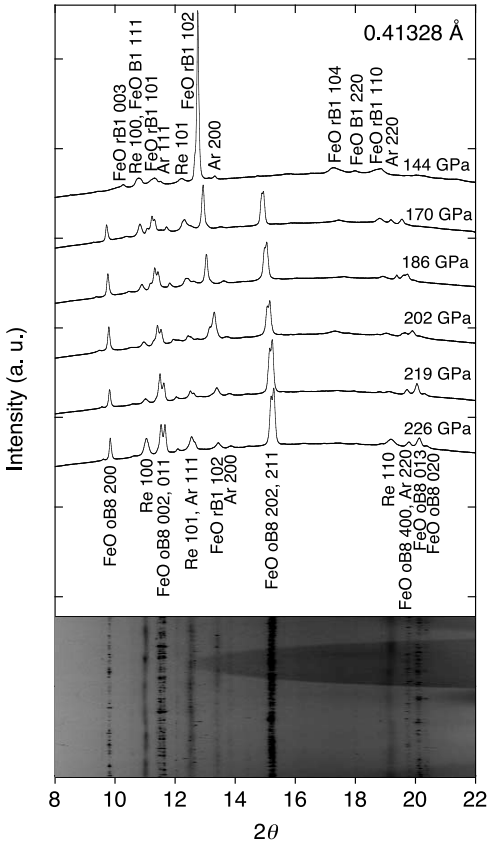

Figure 4. Observed 1D diffraction pattern of $Fe_{0.95}O$ at 144 to 226 GPa, 300 K. Caked 2D diffraction image at 226 GPa is also shown. The B8-type phase was observed above 170 GPa. The peaks from B8 phase can be indexed by slightly distorted orthorhombic unit-cell.

Table 5. Observed and Calculated X-Ray Diffraction Peaks of Orthorhombic B8 Phase of $Fe_{0.95}O$ at 226 GPa[a]

h	k	l	d_{obs}	d_{calc}	Δd
2	0	0	2.40886(18)	2.40705	0.00181
0	0	2	2.05693(23)	2.05658	0.00036
0	1	1	2.03399(20)	2.03386	0.00013
2	0	2	1.56306(19)	1.56359	0.00001
2	1	1	1.55357(15)	1.55353	0.00004
4	0	0	1.20326(9)	1.20353	−0.00027
0	1	3	1.18282(7)	1.18294	−0.00012

[a]Numbers in parentheses represent errors in the last digits. Lattice parameters of a = 4.81411 ± 0.00086 Å, b = 2.33994 ± 0.00088 Å, and c = 4.11315 ± 0.00090 Å were determined by using the UnitCell [*Holland and Redfern*, 1997].

2.048 at 170 GPa to 2.057 at 226 GPa, consistent with the result of *Fei and Mao* [1994].

[18] The B8 FeO should have either normal- (Fe at Ni position and O at As position) or inverse-type structure. The normal B8 phase is possibly metallic, while the inverse structure should be an insulator [e.g., *Fang et al.*, 1999, and references therein]. The normal- and inverse-type B8 structures may be distinguished based on the relative peak intensities. In the present experiments, the combined intensities of 002 and 011 peaks of the oB8 phase and those of 202 and 211 peaks were stronger than those of 102 and 111 peaks; the oB8 102 and 111 peaks overlapped with the Re 101 line, but the overall intensity was still weak (Figure 4). This suggests that the observed oB8 phase is more consistent with the normal type phase. It contrasts with the earlier observations of the B8 phase around 80 GPa by *Kondo et al.* [2004] and *Murakami et al.* [2004].

3.3.2. Compression Curve

[19] The P-V data of the rB1 and oB8 phases at 300 K are illustrated in Figure 5. The observed volume of the rB1

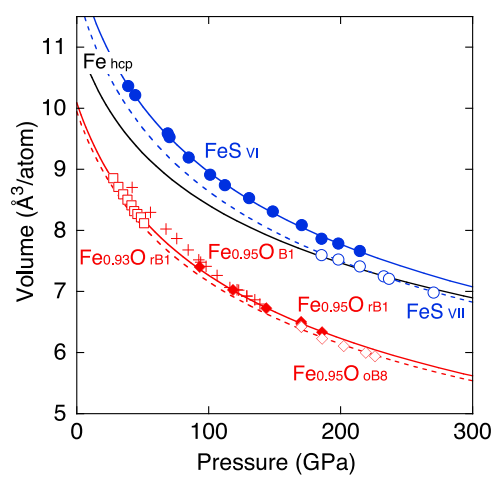

Figure 5. Observed volumes of FeO and FeS. ($Fe_{0.95}O$, red) Closed diamonds and solid curve, rB1 phase; open diamonds and dashed curve, oB8; crosses, B1 at 1500 K. ($Fe_{0.93}O$, red) Open squares, rB1 from *Jacobsen et al.* [2005]. (FeS, blue) Closed circles and solid curve, VI phase from *Ohfuji et al.* [2007]; open circles and dashed curve, VII phase by *Sata et al.* [2008]. Black solid curve represents hcp Fe [*Dubrovinsky et al.*, 2000].

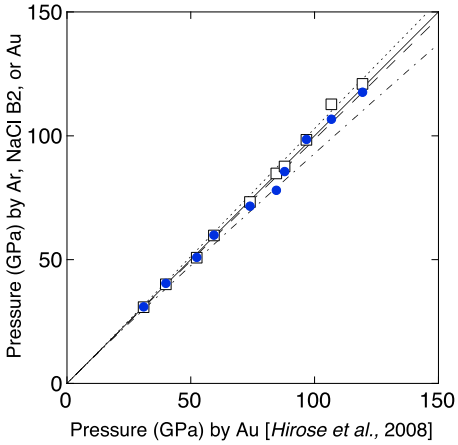

Figure 6. Pressures calculated from Ar [*Jephcoat*, 1998] (blue circles) and B2-NaCl scales [*Sata et al.*, 2002] (open squares), plotted as a function of pressure determined by simultaneously measured volumes of Au and its equation of state [*Hirose et al.*, 2008]. Solid line represents the 1:1 line (Hirose's Au scale). The pressures from different Au scales are shown by dotted line [*Dewaele et al.*, 2004], dashed line [*Heinz and Jeanloz*, 1984], and dash-dotted line [*Shim et al.*, 2002].

phase is consistent with the previous reports by *Shu et al.* [1998] for $Fe_{0.947}O$ and by *Jacobsen et al.* [2005] for $Fe_{0.93}O$. *Ono et al.* [2007b] also reported the *P-V* relations of rB1 phase of $Fe_{0.90}O$ up to 142 GPa with discontinuous volume change of 1.6% at 80–90 GPa; however, their observed volume below 80 GPa was larger by about 2% than that measured in other three studies [*Shu et al.*, 1998; *Jacobsen et al.*, 2005; this study], in spite of the fact that Ono and co-workers measured less stoichiometric (Fe-poor) composition. The volumes obtained by *Ono et al.* [2007b] at pressures higher than 90 GPa are generally consistent with ours.

[20] Present data on rB1 to 186 GPa combined with those by *Jacobsen et al.* [2005] were fitted to the mBM3 EoS, and we obtained $P_r = 0.0 \pm 2.0$ GPa, $K_r = 154 \pm 10$ GPa, and $K'_r = 4.05 \pm 0.20$ with $V_r = 10.113$ Å^3/atom (= 59.161 Å^3/unit-cell). The volume of the oB8 phase was measured between 170 and 226 GPa, but the data are not enough to establish its EoS independently. We therefore assumed $K_0 = 154$ GPa and $K'_0 = 4.04$ same as those of the rB1 phase and obtained only $V_0 = 9.9457 \pm 0.0018$ Å^3/atom (= 77.576 ± 0.015 Å^3/unit-cell) by fitting the data to the BM3 EoS (Figure 3). The fit showed very small errors, indicating that the experimental data are well reproduced by the EoS obtained. Figure 3 illustrates that both rB1 and oB8 are much more compressible than hcp Fe under the core pressures [*Dubrovinsky et al.*, 2000].

[21] $Fe_{0.95}O$ adopted the cubic B1 structure at 1500 K between 42 and 139 GPa. These isothermal compression data are also illustrated in Figure 3. The B1 phase at 1500 K had apparently the same volume per atom with the rB1 phase at room temperature above ~100 GPa. This should be because the pressure for this high-temperature experiment was underestimated possibly by 5 to 10 GPa, because it was determined at 300 K and the contribution of thermal pressure was not taken into account. The B1 phase is indeed much more compressible than the hcp Fe at equivalent pressure and temperature [*Dubrovinsky et al.*, 2000].

3.4. FeS

[22] FeS exhibits a rich polymorphism, and FeS I to VII phases have been reported so far [e.g., *Kavner et al.*, 2001; *Ono and Kikegawa*, 2006; *Sata et al.*, 2008]. All of FeS I to VI phases are closely related to the B8 structure, while only FeS VII phase has cubic B2-type structure. Previous experiments performed by *Ohfuji et al.* [2007] and *Sata et al.* [2008] demonstrated that FeS VI phase is stable above 36 GPa at 300 K and subsequently transforms to FeS VII above 180 GPa. The *P-V* data of these FeS VI and VII phases are summarized in Table 1. Phase transition from FeS VI to VII causes a large volume reduction by about 3% (Figure 5), due to an increase in coordination number from six to eight.

[23] Fitting the data of FeS VI phase to the mBM3 EoS provided $P_r = 36.0 \pm 1.7$ GPa, $K_r = 306 \pm 17$ GPa, and $K'_r = 3.81 \pm 0.28$ with $V_r = 12.615$ cm^3/atom [*Ohfuji et al.*, 2007]. When $V_r = 12.37$ Å^3/atom (98.96 Å/unit-cell) is chosen, $P_r = 0.0 \pm 4.2$ GPa, $K_r = 148 \pm 16$ GPa, and $K'_r = 4.53 \pm 0.34$ are obtained from the same mBM3 EoS. While six data points were collected between 186 and 237 GPa for B2-type FeS VII, they are not enough to determine the EoS independently. We therefore assumed $K_0 = 148$ GPa and $K'_0 = 4.53$ same as those for FeS VI phase and obtained only $V_0 = 11.931 \pm 0.013$ Å^3/atom (= 23.862 ± 0.026 Å^3/unit-cell) by fitting to the BM3 EoS. Note that the volume per atom in B2-type FeS VII is almost the same as that of pure iron at equivalent pressure [*Dubrovinsky et al.*, 2000] (Figure 5). This is consistent with the prediction by theory [*Alfè et al.*, 2002]. Both FeS VI and VII phases are more compressible than pure Fe in the core pressure range.

3.5. Simultaneous Volume Measurements of Ar, Au, MgO, NaCl, and Pt

[24] The volumes of Au, Ar, and B2-type NaCl were simultaneously measured at 300 K in run PM#1 (Table 2). Pressures were calculated from Ar [*Jephcoat*, 1998], B2-NaCl (MgO calibration, mBM3 EoS [*Sata et al.*, 2002]), and Au [*Heinz and Jeanloz*, 1984; *Shim et al.*, 2002; *Dewaele et al.*, 2004; *Hirose et al.*, 2008], and they are plotted as a function of pressure obtained from Hirose's Au (Figure 6). The results show that the Ar and B2-NaCl pressure scales are consistent with each other; the difference is only less than 2 GPa at 119 GPa. The pressures by Ar and NaCl are plotted very closely to 1:1 line in Figure 6, indicating that they match the Au scale by *Hirose et al.* [2008] as well. Note that the Hirose's Au scale is based on the MgO pressure scale proposed by *Speziale et al.* [2001], thus indicating that these Ar and NaCl pressure scales are in good agreement with the MgO scale too.

[25] We also measured the volumes of Pt, Ar, and B2-NaCl at the same time in run PM#2 and those of Pt, MgO, and B2-NaCl in run PM#3 (Table 2). The pressures based on Ar [*Jephcoat*, 1998], B2-NaCl [*Sata et al.*, 2002], and MgO scales [*Speziale et al.*, 2001] were plotted together as a function of pressure by Pt [*Holmes et al.*, 1989] (Figure 7). These results indicate that Jephcoat's Ar pressure scale is consistent with the Holmes's Pt scale within 1.5 GPa at 116 GPa. The Speziale's MgO scale and the Sata's B2-NaCl scale are also in good agreement with the Holmes's Pt scale

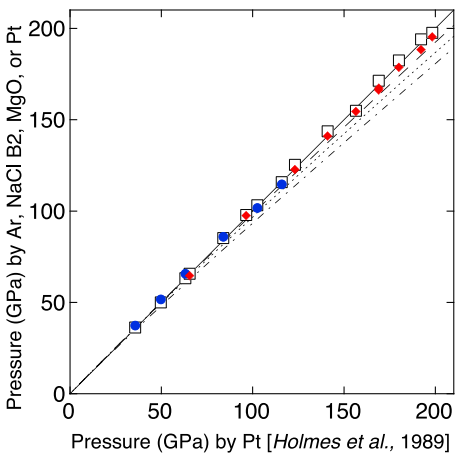

Figure 7. Pressures from Ar [*Jephcoat*, 1998] (blue circles), B2-NaCl [*Sata et al.*, 2002] (open squares), and MgO scales [*Speziale et al.*, 2001] (red diamonds), plotted as a function of pressure based on Pt [*Holmes et al.*, 1989]. Solid line shows the 1:1 line (Holme's Pt scale). The pressures from different Pt scales are given by dashed line [*Dorogokupets and Oganov*, 2007], dotted line [*Dewaele et al.*, 2004], and dash-dotted line [*Zha et al.*, 2008].

even at the core pressure range; the MgO and B2-NaCl give pressures 4 GPa lower and 2 GPa higher than the Pt scale, respectively, around 200 GPa. The Pt scales by *Dorogokupets and Oganov* [2007], *Dewaele et al.* [2004], and *Zha et al.* [2008] are also shown for comparison.

4. Discussion

4.1. Pressure Determination

[26] In the present experiments, pressures were determined by using several different pressure standards; MgO for FeSi and Fe_3C, Ar for $Fe_{0.95}O$ at 300 K, and B2-NaCl for $Fe_{0.95}O$ at high temperature. In addition, both MgO and Ar were used for FeS VI [*Ohfuji et al.*, 2007], and MgO was employed for FeS VII phase [*Sata et al.*, 2008]. The compression behavior of pure Fe was obtained based on the Pt scale [*Dubrovinsky et al.*, 2000]. Furthermore, several different *P-V* EoSs have been proposed for each pressure standard. Depending on the choice of such pressure standard and its EoS, the pressures could be systematically different between the experiments. Indeed, even for a particular pressure standard (material), the different EoSs give different pressures by as much as 10%; for instance, the EoSs of Pt by *Holmes et al.* [1989] and *Zha et al.* [2008] predicts 200 and 180 GPa, respectively, for a certain volume (Figure 7).

[27] While the absolute pressure scale is not available so far, it is important to verify their mutual consistency at high pressure. Present simultaneous volume measurements of these pressure standards up to 198 GPa demonstrate that their *P-V* EoSs used in this study are virtually consistent with each other, at least at room temperature. Our data show that the pressures based on the MgO scale proposed by *Speziale et al.* [2001], Ar scale by *Jephcoat* [1998], B2-NaCl scale by *Sata et al.* [2002], Pt scale by *Holmes et al.* [1989], and Au scale by *Hirose et al.* [2008] are different by only less than 2% at 200 GPa and 300 K (Figures 6 and 7).

4.2. Density of Iron-Light Element Compound

[28] The compression curves of FeSi, Fe_3C, $Fe_{0.95}O$, and FeS are compared with that of hcp Fe in Figures 1 and 5. The *P-T-V* data of hcp Fe reported by *Dubrovinsky et al.* [2000] is used here, since their measurements were made over the widest *P-T* range (up to 300 GPa and 1300 K) and consistent with the shock-wave data within 0.5% in density at the core pressures [*Brown and McQueen*, 1986]. More recent volume measurements by *Dewaele et al.* [2006] and *Nishio-Hamane et al.* [2010] were conducted only at room temperature. The V_0, K_0, and K'_0 for these iron compounds determined in this study are summarized in Table 6. Note that hcp Fe has higher K'_0 than any iron–light element compounds measured in this study, resulting in that iron becomes less compressible under the Earth's core pressures.

[29] In order to look the compressibility more closely, here we consider the partial volume of light element X in Fe-X compound relative to the volume of iron in hcp structure (V_X/V_{Fe}). V_X/V_{Fe} is defined as:

$$V_{Fe-X} = V_{Fe}\left[(1-x) + x \cdot \frac{V_X}{V_{Fe}}\right] \quad (3)$$

where $V_{Fe\text{-}X}$ and V_{Fe} are the volumes of measured Fe-X compound and pure iron, respectively, and x is an atomic ratio of X in Fe-X compound (x = 0.5128 for $Fe_{0.95}O$, 0.25 for Fe_3C, and 0.5 for FeSi and FeS). V_X/V_{Fe} is estimated for each light element as a function of pressure from each measured *P-V* datum of iron-compound and from its EoS (Table 1 and Figure 8). Only V_S/V_{Fe} value is greater than a unit, meaning that the partial volume of sulfur in FeS VI is larger than the volume of iron in the hcp structure. In the same sense, the partial volumes of both S in FeS VII and Si in B2-type FeSi are very similar to the volume of Fe. On the other hand, those of O in $Fe_{0.95}O$ and C in Fe_3C are substantially smaller than that of Fe.

[30] At pressures less than ~100 GPa, the V_X/V_{Fe} values of O and S decrease with increasing pressure, whereas those of Si and C increase with pressure (Figure 8). It reflects the fact that ionic compounds of $Fe_{0.95}O$ and FeS are more compressible than pure Fe, while non-ionic compounds FeSi and Fe_3C are less compressible than Fe at relatively low pressures. Nevertheless, at pressures greater than 100 GPa, the V_X/V_{Fe} values for all of these light elements decrease with increasing pressure, demonstrating that both ionic and non-ionic iron compounds have larger compressibilities than hcp Fe at pressures corresponding to the Earth's core (>135 GPa). In addition, the *P-V* data of FeH_x have been

Table 6. List of Parameters for the Third Order Birch-Murnaghun Equations of State for Iron Compounds

	hcp Fe[a]	FeSi	Fe_3C	$Fe_{0.95}O$ rB1	$Fe_{0.95}O$ oB8	FeS VI	FeS VII
V_0 (Å^3/atom)	11.2	10.685	9.341	10.113	9.9457	12.37	11.931
K_0(GPa)	155.6	221.7	290	154	154[a]	148	148[b]
K'_0	5.81	4.167	3.76	4.04	4.04[a]	4.53	4.53[b]

[a]*Dubrovinsky et al.* [2000].
[b]Fixed value.

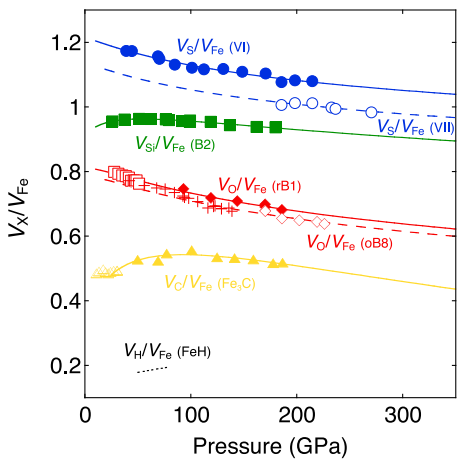

Figure 8. V_X/V_{Fe} for Si (green), C (yellow), O (red), and S (blue). Si, estimated from B2-FeSi (squares); C, from Fe_3C (triangles); O, from rB1 $Fe_{0.95}O$ (closed diamonds, solid curve), oB8 $Fe_{0.95}O$ (open diamonds, dashed curve), B1 $Fe_{0.95}O$ (at 1500 K, crosses), and rB1 $Fe_{0.93}O$ (open squares); S, from FeS VI (closed circles, solid curve) and VII phases (open circles, dashed curve). Dotted curve indicates the data for H from FeH [*Hirao et al.*, 2004]. Note that V_X/V_{Fe} for Si, C, O, and S has negative slope above ~100 GPa, indicating that the incorporation of these light elements in iron enhances the compressibility.

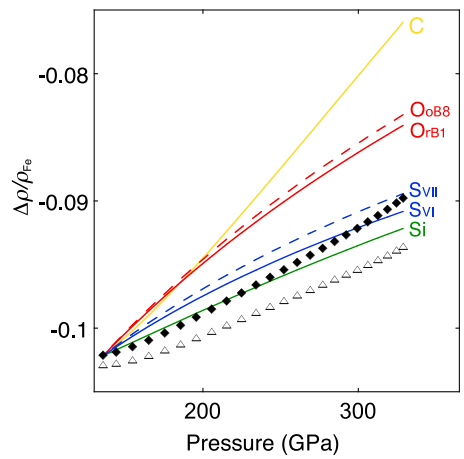

Figure 9. Density deficit of the Earth model, PREM, relative to iron ($\Delta\rho_{PREM}/\rho_{Fe}$) and change in that of hypothetical iron compounds ($\Delta\rho_{Fe\text{-}X}/\rho_{Fe}$) along the core *P-T* profile. Composition of the compounds is fixed to the estimated value, that is explained the density at the CMB. $\Delta\rho_{PREM}/\rho_{Fe}$: diamonds, based on parameters of *Stacey* [1994]; triangles, *Boehler et al.* [1995]. $\Delta\rho_{Fe\text{-}X}/\rho_{Fe}$: C, $Fe_{0.72}C_{0.28}$; O_{oB8}, $Fe_{0.76}O_{0.24}$; O_{rB1}, $Fe_{0.77}O_{0.23}$; S_{VII}, $Fe_{0.78}S_{0.22}$; S_{VI}, $Fe_{0.80}S_{0.20}$,; Si, $Fe_{0.77}Si_{0.23}$. Note that density deficits both of $Fe_{0.77}Si_{0.23}$ and $Fe_{0.78\text{-}0.80}S_{0.22\text{-}0.20}$ match $\Delta\rho_{PREM}/\rho_{Fe}$ in the whole outer core, while $Fe_{0.76\text{-}0.77}O_{0.24\text{-}0.23}$ and $Fe_{0.72}C_{0.28}$ have much higher densities than the PREM at the ICB.

also reported up to 80 GPa [*Hirao et al.*, 2004]. Hirao and others observed that FeH_x became less compressible above 50 GPa than at lower pressures, possibly due to the magnetic transition. We calculated V_H/V_{Fe} from *Hirao et al.* [2004] between 50 and 80 GPa in Figure 8. Note that V_H/V_{Fe} has a positive pressure effect, indicating that it is less compressible than pure iron, at least in such a limited pressure range.

4.3. Identification of Light Element in the Core

[31] Here we try to identify the light element in the outer core based on the density and compressibility of iron–light element compound. The density deficit of a hypothetical iron compound ($\Delta\rho_{Fe\text{-}X}/\rho_{Fe}$) at 300 K is estimated as a function of pressure from equation (A2) in Appendix A. The deficit at core temperature should be discussed, but the thermal expansivity at the core *P-T* is not known yet. We thus assume that the thermal expansivities of iron compounds are the same as that of pure Fe, meaning that the density deficit at 300 K is identical to that at high temperature.

[32] We also calculate $\Delta\rho_{PREM}/\rho_{Fe}$ from the preliminary reference Earth model (PREM) [*Dziewonski and Anderson*, 1981] and the density of hcp Fe along the core *P-T* profile [*Dubrovinsky et al.*, 2000], according to the procedure described in Appendix B. The results are shown in Figure 9. The calculation shows that the density of the Earth's outer core is smaller by about 10% than pure iron. It is noted that the outer core $\Delta\rho_{PREM}/\rho_{Fe}$ increases very mildly with increasing pressure, indicating that the outer core has slightly higher compressibility than pure iron along the adiabat. This is indeed consistent with the fact that the incorporation of light element enhances the compressibility of iron (Figure 8). The inner core is almost constantly lighter than pure iron by 4.5% for temperature modeled by *Stacey* [1994] or 4.9% for that of *Boehler et al.* [1995].

[33] Now we estimate the abundance, *x*, of light element by comparing $\Delta\rho_{Fe\text{-}X}/\rho_{Fe}$ with $\Delta\rho_{PREM}/\rho_{Fe}$, when the core contains single light alloying element (this represents the maximum abundance). The results are shown in Figure 10. The maximum contents in the outer core are calculated to be 28–32 atm% for C, 22.5–23.9 atm% for O (based on the rB1

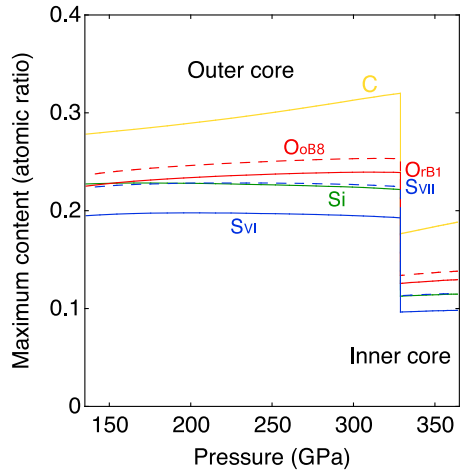

Figure 10. The abundance of O, C, Si, and S required to account for the core density deficit as a single light element. Note that required C and O contents increase with increasing pressure, inconsistent with the chemically uniform liquid outer core.

phase), 22.2–22.7 atm% for Si, and 19.3–19.5 atm% for S (based on the FeS VI phase) in atomic ratios. *Jeanloz and Ahrens* [1980] performed shock-wave experiments on $Fe_{0.94}O$ up to 228 GPa and compared its density with those of Fe [*McQueen et al.*, 1970] and the outer core [*Dziewonski et al.*, 1975; *Anderson and Hart*, 1976]. After thermal correction, Jeanloz and Ahrens proposed 28 atm% (10 wt%) oxygen to account for the outer core density, consistent with our current estimate. Similarly *Poirier* [1994] demonstrated that the 10% density deficit in the outer core is reconciled either with 26 atm% (9 wt%) O, 18 atm% (11 wt%) S, or 30 atm% (18 wt%) Si, based on the shock-wave data of Fe [*Brown and McQueen*, 1982], $Fe_{0.94}O$ [*Jeanloz and Ahrens*, 1980], $Fe_{0.9}S$ [*Brown et al.*, 1984], and Fe-19.8wt%Si ($Fe_{0.67}Si_{0.33}$) [*Balchan and Cowan*, 1966].

[34] The liquid outer core is most likely homogeneous in composition due to its vigorous convection. However, if carbon is a single light element in the core, its abundance needs to increase from 27.8 atm% at the core-mantle boundary (CMB) to 32.0 atm% at the ICB, which is inconsistent with the chemically uniform outer core. Similarly, the required O abundance increases from 22.5 atm% at the CMB to 23.9 atm% at the ICB. These suggest that both C and O are unlikely to be a predominant light element in the core. The previous estimations by *Jeanloz and Ahrens* [1980] and *Poirier* [1994] did not consider such chemical homogeneity in the outer core.

[35] The substitution of light element in iron not only reduces the density but also enhances the compressibility. Every light element explains the $\Delta\rho_{PREM}/\rho_{Fe}$ at a single depth but not the $\Delta\rho_{PREM}/\rho_{Fe}$ profile in the whole outer core. Assuming a sole light element in the core, we first estimate the abundance of C, O, Si, and S required to account for $\Delta\rho_{PREM}/\rho_{Fe}$ at the CMB; $Fe_{0.72}C_{0.28}$, $Fe_{0.76\text{-}0.77}O_{0.24\text{-}0.23}$, $Fe_{0.77}Si_{0.23}$, and $Fe_{0.78\text{-}0.80}S_{0.22\text{-}0.20}$. With these compositions fixed, the change in $\Delta\rho_{Fe\text{-}X}/\rho_{Fe}$ with increasing pressure is calculated for each composition (Figure 9). We found that $\Delta\rho_{Fe\text{-}X}/\rho_{Fe}$ for both $Fe_{0.77}Si_{0.23}$ and $Fe_{0.78\text{-}0.80}S_{0.22\text{-}0.20}$ match $\Delta\rho_{PREM}/\rho_{Fe}$ in the whole outer core. In contrast, the densities of $Fe_{0.76\text{-}0.77}O_{0.24\text{-}0.23}$ and $Fe_{0.72}C_{0.28}$ are identical to the PREM density at the CMB but are much larger at the ICB. These suggest that both C and O are not plausible as a predominant light element in the core, leaving Si and S as strong candidates.

4.4. Limitation of Current Estimates

[36] While the Earth's outer core is molten, the effect of light element is estimated from the experimental results on solids. First we assumed the same volume for solid and liquid iron, which overestimates the core density deficit ($\Delta\rho_{PREM}/\rho_{Fe}$). Nevertheless, their volume difference was previously found to be very small at core pressures, less than 1% around 250 GPa on shock wave Hugoniot [*Brown*, 2001]. More importantly, the effect of non-ideal volume mixing between iron and light element was not considered here but may be important for liquid. Indeed, thermodynamical modeling by *Helffrich and Kaneshima* [2004] suggested a large volume mixing non-ideality in liquid Fe-FeS. This changes the estimates of $\Delta\rho_{Fe\text{-}X}/\rho_{Fe}$, but obviously we need more information on the properties of liquid iron and iron compounds in order to include this effect properly.

[37] We obtained V_X/V_{Fe} from the volumes of iron compounds, but the volume depends on the crystal structure (Figure 8). FeS, for example, reduces its volume by about 3% upon transformation from VI to VII phase around 200 GPa [*Sata et al.*, 2008], and hence V_S/V_{Fe} decreases by 0.07. Nevertheless, the compressibilities of FeS VI and VII are comparable at relevant pressure range. Thus, it changes the estimate of possible S content in the core (Figure 10) but affects our argument on the compressibility little (Figure 9). This is the same for O as well. Furthermore, V_X/V_{Fe} is assumed to be invariable with temperature. This assumption is partly supported by the previous experiments by *Seagle et al.* [2006], which demonstrated that Fe and Fe_3S have identical thermal expansivity up to 80 GPa and 2500 K. The substitution of silicon in iron also does not change the thermoelastic properties of Fe-Si alloys [*Zhang and Guyot*, 1999]. Our data on $Fe_{0.95}O$ demonstrate that the V_O/V_{Fe} values are similar but slightly lower at 1500 K than at 300 K (Figure 8). This is in part due to the underestimation of pressure in high-temperature experiments, but it is still true that ionic $Fe_{0.95}O$ has smaller thermal expansivity than metallic Fe [*Seagle et al.*, 2008]. This is not critical, however, as far as the pressure effect on thermal expansivity of $Fe_{0.95}O$ is comparable to that on Fe at sufficiently high pressures.

[38] Sound velocity data can independently constrain the composition of the Earth's core. *Badro et al.* [2007] reported sound velocity measurements on FeO, FeSi, FeS, and FeS_2, suggesting that sulfur is not likely the important light element in the Earth's core. Nevertheless, such velocity data of Fe compounds were obtained below 90 GPa and extrapolated to core conditions based on the Birch's law (sound velocity is a linear function of density). The validity of such Birch's law at high temperature has been controversial [*Lin et al.*, 2005].

[39] Finally, these results also suggest the coexistence of liquid $Fe_{0.78}Si_{0.22}$ and solid $Fe_{0.89}Si_{0.11}$ or liquid $Fe_{0.78\text{-}0.81}S_{0.22\text{-}0.19}$ and solid $Fe_{0.89\text{-}0.90}S_{0.11\text{-}0.10}$ at the ICB (Figure 10), if Si or S is a sole light element in the core. However, these compositions of coexisting liquid and solid are not consistent with those expected from the Fe-Si and Fe-S phase diagrams experimentally determined so far at relatively low *P-T*. The compositional difference between the coexisting liquid and solid is very small in Fe-FeSi system, at least at 21 GPa [*Kuwayama and Hirose*, 2004]. Regarding the sulfur, *Stewart et al.* [2007] has demonstrated that iron-rich Fe-S liquid crystallizes iron with limited amount of sulfur up to 40 GPa. Nevertheless, the partitioning of light elements between the solid and liquid phases may change dramatically at higher *P-T* conditions corresponding to the Earth's core, as predicted by theory [*Alfè et al.*, 2002]. Such information provides further constraints on the identification of light element in the core.

Appendix A: Density Estimation of Hypothetical Iron Compound

[40] Under the assumption of ideal volume mixing between pure iron and each light element, the volume of hypothetical iron compound ($V_{Fe\text{-}X}$) containing specific amount of light element X is calculated using equation (3). The mass ratio m_X/m_{Fe} is similarly calculated from that of

Fe, Si, C, O, and S; m_{Si}/m_{Fe} = 0.5029, m_C/m_{Fe} = 0.2151, m_O/m_{Fe} = 0.2865, and m_S/m_{Fe} = 0.5742. They have no pressure and temperature dependence. The density of a hypothetical mixture $Fe_{1-x}X_x$ is subsequently calculated as:

$$\rho_{Fe-X} \equiv \rho_{Fe}\left(1+\frac{\Delta\rho_{Fe-X}}{\rho_{Fe}}\right) = \frac{m_{Fe-X}}{V_{Fe-X}} = \frac{m_{Fe}\left[(1-x)+x\cdot\frac{m_X}{m_{Fe}}\right]}{V_{Fe}\left[(1-x)+x\cdot\frac{V_X}{V_{Fe}}\right]} \quad \text{(A1)}$$

where ρ_{Fe} is the density of iron. The density deficit of $Fe_{1-x}X_x$ compound relative to iron, $\Delta\rho_{Fe-X}/\rho_{Fe}$, is given by V_X/V_{Fe}, and x:

$$\frac{\Delta\rho_{Fe-X}}{\rho_{Fe}} = \frac{\left[(1-x)+x\cdot\frac{m_X}{m_{Fe}}\right]}{\left[(1-x)+x\cdot\frac{V_X}{V_{Fe}}\right]} - 1. \quad \text{(A2)}$$

Appendix B: Estimation of Core Density Deficit From Pure Iron

[41] We calculate $\Delta\rho_{PREM}/\rho_{Fe}$ from the preliminary reference Earth model (PREM) [*Dziewonski and Anderson*, 1981] and the density of hcp Fe along the core *P-T* profile [*Dubrovinsky et al.*, 2000]. The density difference between solid and liquid iron is practically small at the core pressure range (<1%) [*Brown*, 2001] and is thus not considered here. Temperature at the inner core boundary (ICB) has been inferred from the melting temperature of iron, which was found to be 5600 to 6500 K in the literature [*Anderson and Duba*, 1997]. Here we adopt 5300 K as the ICB temperature, considering a reduction of melting temperature by 500–1000 K due to the addition of light element. The adiabatic temperature gradient in the outer core is relatively well known [*Stacey*, 1994]. The inner core temperature is assumed to be constant (this means no internal heat source). Additionally, the relatively low ICB temperature of 4850 K and the small temperature gradient proposed by *Boehler et al.* [1995] are also considered.

[42] **Acknowledgments.** We thank anonymous referees for valuable comments which helped to improve the manuscript. The synchrotron X-ray diffraction experiments were conducted at SPring-8 (proposal 2006B0099, 2007A0099, 2007B0099, 2008A0099, 2008B0099, and 2009A0087) and Advanced Photon Source (proposal G000338). This work was partially supported by the JSPS research grant.

References

Alfè, D., M. J. Gillan, and G. D. Price (2002), Composition and temperature of the Earth's core constrained by combining ab initio calculations and seismic data, *Earth Planet. Sci. Lett.*, *195*, 91–98.

Anderson, D. L., and R. S. Hart (1976), An Earth model based on free oscillations and body waves, *J. Geophys. Res.*, *81*, 1461–1475.

Anderson, O. L., and A. Duba (1997), Experimental melting curve of iron revisited, *J. Geophys. Res.*, *102*, 22,659–22,669.

Badro, J., G. Fiquet, F. Guyot, E. Gregoryanz, F. Occelli, D. Antonangeli, and M. d'Astuto (2007), Effect of light elements on the sound velocities in solid iron: Implications for the composition of Earth's core, *Earth Planet. Sci. Lett.*, *254*, 233–238, doi:10.1016/j.epsl.2006.11.025.

Balchan, A. S., and G. R. Cowan (1966), Shock compression of two iron-silicon alloys to 2.7 megabars, *J. Geophys. Res.*, *71*, 3577–3588.

Birch, F. (1952), Elasticity and constitution of the Earth's interior, *J. Geophys. Res.*, *57*, 227–284.

Birch, F. (1986), Equation of state and thermodynamic parameters of NaCl to 300 kbar in the high-temperature domain, *J. Geophys. Res.*, *91*, 4949–4954.

Boehler, R., A. Chopelas, and A. Zerr (1995), Temperature and chemistry of the core-mantle boundary, *Chem. Geol.*, *120*, 199–205.

Brown, J. M. (2001), Equation of state of iron to 450 GPa: Another high pressure solid phase?, *Geophys. Res. Lett.*, *28*, 4339–4342.

Brown, J. M., and R. G. McQueen (1982), The equation of state for iron and the Earth's core, in *High-Pressure Research in Geophysics*, edited by S. Akimoto and M. H. Manghnani, pp. 611–623, Cent. for Acad. Publ. Jpn., Tokyo.

Brown, J. M., and R. G. McQueen (1986), Phase transition, Grüneisen parameter, and elasticity for shocked iron between 77 GPa and 400 GPa, *J. Geophys. Res.*, *91*, 7485–7494.

Brown, J. M., T. J. Ahrens, and D. L. Shampine (1984), Hugoniot data for pyrrhotite and the Earth's core, *J. Geophys. Res.*, *89*, 6041–6048.

Campbell, A. J., L. Danielson, K. Righter, C. T. Seagle, Y. Wang, and V. B. Prakapenka (2009), High pressure effects on the iron-iron oxide and nickel-nickel oxide oxygen fugacity buffers, *Earth Planet. Sci. Lett.*, *286*, 556–564, doi:10.1016/j.epsl.2009.07.022.

Caracas, R., and R. Wentzcovitch (2004), Equation of state and elasticity of FeSi, *Geophys. Res. Lett.*, *31*, L20603, doi:10.1029/2004GL020601.

Dewaele, A., P. Loubeyre, and M. Mezouar (2004), Equations of state of six metals above 94 GPa, *Phys. Rev. B*, *70*, 094112, doi:10.1103/PhysRevB.70.094112.

Dewaele, A., P. Loubeyre, F. Occelli, M. Mezouar, P. I. Dorogokupets, and M. Torrent (2006), Quasihydrostatic equation of state of iron above 2 Mbar, *Phys. Rev. Lett.*, *97*, 215504, doi:10.1103/PhysRevLett.97.215504.

Dobson, D. P., L. Vočadlo, and I. G. Wood (2002), A new high-pressure phase of FeSi, *Am. Mineral.*, *87*, 784–787.

Dobson, D. P., W. A. Crichton, P. Bouvier, L. Vočadlo, and I. G. Wood (2003), The equation of state of CsCl-structured FeSi to 40 GPa: Implications for silicon in the Earth's core, *Geophys. Res. Lett.*, *30*(1), 1014, doi:10.1029/2002GL016228.

Dorogokupets, P. I., and A. R. Oganov (2007), Ruby, metals, and MgO as alternative pressure scales: A semiempirical description of shock-wave, X-ray, and thermochemical data at high temperatures and pressures, *Phys. Rev. B*, *75*, 024115, doi:10.1103/PhysRevB.75.024115.

Dubrovinsky, L. S., S. K. Saxena, F. Tutti, S. Rekhi, and T. Le Behan (2000), In situ X-ray study of thermal expansion and phase transition of iron at multimegabar pressure, *Phys. Rev. Lett.*, *84*, 1720–1723, doi:10.1103/PhysRevLett.84.1720.

Dziewonski, A. M., and D. L. Anderson (1981), Preliminary reference Earth model, *Phys. Earth Planet. Inter.*, *25*, 297–356.

Dziewonski, A. M., A. L. Hales, and E. R. Lapwood (1975), Parametrically simple Earth models consistent with geophysical data, *Phys. Earth Planet. Inter.*, *10*, 12–48.

Fang, Z., I. V. Solovyev, H. Sawada, and K. Terakura (1999), First-principles study on electronic structures and phase stability of MnO and FeO under high pressure, *Phys. Rev. B*, *59*, 762–774.

Fei, Y., and H.-K. Mao (1994), In situ determination of the NiAs phase of FeO at high pressure and temperature, *Science*, *266*, 1678–1680.

Hammersley, A. P., S. O. Svensson, M. Hanfland, A. N. Fitch, and D. Häusermann (1996), Two-dimensional detector software: From real detector to idealized image or two-theta scan, *High Pressure Res.*, *14*, 235–248.

Heinz, D. L., and R. Jeanloz (1984), The equation of state of the gold calibration standard, *J. Appl. Phys.*, *55*, 885–893.

Helffrich, G., and S. Kaneshima (2004), Seismological constraints on core composition from Fe-O-S liquid immiscibility, *Science*, *306*, 2239–2242, doi:10.1126/science.1101109.

Hirao, H., T. Kondo, E. Ohtani, K. Takemura, and T. Kikegawa (2004), Compression of iron hydride to 80 GPa and hydrogen in the Earth's inner core, *Geophys. Res. Lett.*, *31*, L06616, doi:10.1029/2003GL019380.

Hirose, K., N. Sata, T. Komabayashi, and Y. Ohishi (2008), Simultaneous volume measurements of Au and MgO to 140 GPa and thermal equation of state of Au based on the MgO pressure scale, *Phys. Earth Planet. Inter.*, *167*, 149–154, doi:10.1016/j.pepi.2008.03.002.

Holland, T. J. B., and S. A. T. Redfern (1997), Unit-cell refinement from powder diffraction data: the use of regression diagnostics, *Mineral. Mag.*, *61*, 65–77.

Holmes, N. C., J. A. Moriarty, G. R. Gathers, and W. J. Nellis (1989), The equation of state of platinum to 660 GPa (6.6 Mbar), *J. Appl. Phys.*, *66*, 2962–2967.

Jacobsen, S. D., J.-F. Lin, R. J. Angel, G. Shen, V. B. Prakapenka, P. Dera, H.-K. Mao, and R. J. Hemley (2005), Single-crystal synchrotron x-ray diffraction study of wüstite and magnesiowüstite at lower-mantle pressures, *J. Synchrotron Radiat.*, *12*, 577–583, doi:10.1107/S0909049505022326.

Jeanloz, R. (1981), Finite-strain equation of state for high-pressure phases, *Geophys. Res. Lett.*, *8*, 1219–1222.
Jeanloz, R., and T. J. Ahrens (1980), Equations of state of FeO and CaO, *Geophys. J. R. Astron. Soc.*, *62*, 505–528.
Jephcoat, A. P. (1998), Rare-gas solids in the Earth's deep interior, *Nature*, *393*, 355–358.
Kavner, A., T. S. Duffy, and G. Shen (2001), Phase stability and density of FeS at high pressures and temperatures: Implications for the interior structure of Mars, *Earth Planet. Sci. Lett.*, *185*, 25–33.
Knittle, E., and Q. Williams (1995), Static compression of ε-FeSi and an evaluation of reduced silicon as a deep Earth constituent, *Geophys. Res. Lett.*, *22*, 445–448.
Kondo, T., E. Ohtani, N. Hirao, T. Yagi, and T. Kikegawa (2004), Phase transitions of (Mg,Fe)O at megabar pressures, *Phys. Earth Planet. Inter.*, *143–144*, 201–213, doi:10.1016/j.pepi.2003.10.008.
Kuwayama, Y., and K. Hirose (2004), Phase relations in the system Fe-FeSi at 21 GPa, *Am. Mineral.*, *89*, 273–276.
Li, J., and Y. Fei (2003), Experimental constraints on core composition, in *Treatise on Geochemistry*, vol. 2, *The Mantle and Core*, edited by R. W. Carlson, pp. 521–546, Elsevier-Pergamon, Oxford, U. K.
Li, J., H. K. Mao, Y. Fei, E. Gregoryanz, M. Eremets, and C. S. Zha (2002), Compression of Fe_3C to 30 GPa at room temperature, *Phys. Chem. Miner.*, *29*, 166–169, doi:10.1007/s00269-001-0224-4.
Lin, J.-F., A. J. Campbell, D. L. Heinz, and G. Shen (2003), Static compression of iron-silicon alloys: Implications for silicon in the Earth's core, *J. Geophys. Res.*, *108*(B1), 2045, doi:10.1029/2002JB001978.
Lin, J.-F., V. V. Struzhkin, H.-K. Mao, R. J. Hemley, P. Chow, M. Y. Hu, and J. Li (2004), Magnetic transition in compressed Fe_3C from X-ray emission spectroscopy, *Phys. Rev. B*, *70*, 212405, doi:10.1103/PhysRevB.70.212405.
Lin, J.-F., W. Sturhahn, J. Zhao, G. Shen, H.-K. Mao, and R. J. Hemley (2005), Sound velocities of hot dense iron: Birch's law revisited, *Science*, *308*, 1892–1894.
McQueen, R. G., S. P. Marsh, J. W. Taylor, J. N. Fritz, and W. J. Carter (1970), The equation of state of solid from shock wave studies, in *High Velocity Impact Phenomena*, edited by R. Kinslow, pp. 294–419, Academic, New York.
Murakami, M., K. Hirose, S. Ono, T. Tsuchiya, M. Isshiki, and T. Watanuki (2004), High pressure and high temperature phase transitions of FeO, *Phys. Earth Planet. Inter.*, *146*, 273–282, doi:10.1016/j.pepi.2003.06.011.
Nishio-Hamane, D., T. Yagi, N. Sata, T. Fujita, and T. Okada (2010), No reactions observed in Xe-Fe system even at Earth core pressures, *Geophys. Res. Lett.*, *37*, L04302, doi:10.1029/2009GL041953.
Ohfuji, H., N. Sata, H. Kobayashi, Y. Ohishi, K. Hirose, and T. Irifune (2007), A new high-pressure and high-temperature polymorph of FeS, *Phys. Chem. Miner. 34*, 335–343, doi:10.1007/s00269-007-0151-0.
Ohishi, Y., N. Hirao, N. Sata, K. Hirose, and M. Takata (2008), Highly intense monochromatic X-ray diffraction facility for high-pressure research at SPring-8, *High Pressure Res.*, *28*, 163–173, doi:10.1080/0895795080228910.
Ono, S., and T. Kikegawa (2006), High-pressure study of FeS between 20 and 120 GPa using synchrotron X-ray powder diffraction, *Am. Mineral.*, *91*, 1941–1944.
Ono, S., T. Kikegawa, and Y. Ohishi (2007a), Equation of state of the high-pressure polymorph of FeSi to 67 GPa, *Eur. J. Mineral.*, *19*, 183–187, doi:10.1127/0935-1221/2007/0019-1713.
Ono, S., Y. Ohishi, and T. Kikegawa (2007b), High-pressure study of rhombohedral iron oxide, FeO, at pressures between 41 and 142 GPa, *J. Phys. Condens. Matter*, *19*, 036205, doi:10.1088/0953-8984/19/3/036205.
Ozawa, H., K. Hirose, S. Tateno, N. Sata, and Y. Ohishi (2010), Phase transition boundary between B1 and B8 structures of FeO up to 210 GPa, *Phys. Earth Planet. Inter.*, *179*, 157–163, doi:10.1016/j.pepi.2009.11.005.
Poirier, J.-P. (1994), Light elements in the Earth's outer core: A critical review, *Phys. Earth Planet. Inter.*, *85*, 319–337.
Sata, N., G. Shen, M. L. Rivers, and S. R. Sutton (2002), Pressure-volume equation of state of the high-pressure B2 phase of NaCl, *Phys. Rev. B*, *65*, 104114, doi:10.1103/PhysRevB.65.104114.
Sata, N., H. Ohfuji, K. Hirose, H. Kobayashi, Y. Ohishi, and N. Hirao (2008), *Am. Mineral.*, *93*, 492–494, doi:10.2138/am.2008.2762.
Scott, H. P., Q. Williams, and E. Knittle (2001), Stability and equation of state of Fe_3C to 73 GPa: Implications for carbon in the Earth's core, *Geophys. Res. Lett.*, *28*, 1875–1878.
Seagle, C. T., A. J. Campbell, D. L. Heinz, G. Shen, and V. B. Prakapenka (2006), Thermal equation of state of Fe_3S and implications for sulfur in Earth's core, *J. Geophys. Res.*, *111*, B06209, doi:10.1029/2005JB004091.
Seagle, C. T., D. L. Heinz, A. J. Campbell, V. B. Prakapenka, and S. T. Wanless (2008), Melting and thermal expansion in the Fe-FeO system at high pressure, *Earth Planet. Sci. Lett.*, *265*, 655–665, doi:10.1016/j.epsl.2007.11.004.
Shen, G., R. L. Rivers, Y. Wang, and S. R. Sutton (2001), Laser heated diamond cell system at the Advanced Photon Source for in situ X-ray measurements at high pressure and temperature, *Rev. Sci. Instrum.*, *72*, 1273–1282, doi:10.1063/1.1343867.
Shim, S.-H., T. S. Duffy, and K. Takemura (2002), Equation of state of gold and its application to the phase boundaries near 660 km depth in Earth's mantle, *Earth Planet. Sci. Lett.*, *203*, 729–739.
Shu, J., H.-K. Mao, J. Hu, Y. Fei, and R. J. Hemley (1998), Single-crystal X-ray diffraction of wüstite to 30 GPa hydrostatic pressure, *N. Jahrb. Miner. Abh.*, *172*, 309–323.
Speziale, S., C.-S. Zha, T. S. Duffy, R. J. Hemley, and H.-K. Mao (2001), Quasi-hydrostatic compression of magnesium oxide to 52 GPa: Implications for the pressure-volume-temperature equation of state, *J. Geophys. Res.*, *106*, 515–528.
Stacey, F. (1994), Thermodynamic relationship and the properties of iron at Earth's core conditions, in *High-Pressure Science and Technology-1993*, edited by S. C. Schmidt et al., *AIP Conf. Proc.*, 309, 899–902.
Stewart, A. J., M. W. Schmidt, W. van Westrenen, and C. Liebske (2007), Mars: A new core-crystallization regime, *Science*, *316*, 1323–1325, doi:10.1126/science.1140549.
Vinet, P., J. Ferrante, J. R. Smith, and J. H. Rose (1986), A universal equation of state for solids, *J. Phys. C Solid State Phys.*, *19*, L467–L473.
Vočadlo, L., G. D. Price, and I. G. Wood (1999), Crystal structure, compressibility and possible phase transitions in ε-FeSi studied by first-principles pseudopotential calculations, *Acta Cryst., B55*, 484–493.
Vočadlo, L, J. Brodholt, D. P. Dobson, K. S. Knight, W. G. Marshall, G. D. Price, and I. G. Wood (2002), The effect of ferromagnetism on the equation of state of Fe_3C studied by first-principles calculations, *Earth Planet. Sci. Lett.*, *203*, 567–575.
Zha, C.-S., K. Mibe, W. A. Bassett, O. Tschauner, H.-K. Mao, and R. J. Hemley (2008), P-V-T equation of state of platinum to 80 GPa and 1900 K from internal resistive heating/X-ray diffraction measurements, *J. Appl. Phys.*, *103*, 054908, doi:10.1063/1.2844358.
Zhang, J., and F. Guyot (1999), Thermal equation of state of iron and $Fe_{0.91}Si_{0.09}$, *Phys. Chem. Miner.*, *26*, 206–211.

N. Hirao and Y. Ohishi, SPring-8, Japan Synchrotron Radiation Research Institute, 1-1-1 Koto, Sayo, Hyogo 679-5198, Japan.
K. Hirose, Department of Earth and Planetary Sciences, Tokyo Institute of Technology, 2-12-1 Ookayama, Meguro-ku, Tokyo 152-8551, Japan. (kei@geo.titech.ac.jp)
Y. Nakajima, Bayerishes Geoinstitut, Universität Bayreuth, Universitätsstraße 30, D-95447 Bayreuth, Germany.
N. Sata, Institute for Research on Earth Evolution, Japan Agency for Marine-Earth Science and Technology, 2-15 Natsushima, Yokosuka, Kanagawa, 237-0061, Japan. (n_sata@mac.com)
G. Shen, High Pressure Collaborative Access Team, Geophysical Laboratory, Carnegie Institution of Washington, Bldg. 434E, Argonne, IL 60439, USA.